Arabian Journal of Geosciences (2019) 12: 614
https://doi.org/10.1007/s12517-019-4824-z

ORIGINAL PAPER

Study on the mechanisms and prevention of water inrush events in a deeply buried high-pressure coal seam—a case study of the Chensilou Coal Mine in China

Xianzhi Shi[1] · Shuyun Zhu[1] · Weiqiang Zhang[1]

Received: 30 January 2019 / Accepted: 5 September 2019 / Published online: 11 October 2019

Abstract
Coal mine formations are becoming increasingly threatened by water inrush accidents resulting from high-pressure water conditions in limestone formations below mines with increasingly greater mining depths. This paper focuses on the floor of a deeply buried coal seam and the high-pressure fully mechanized mining faces of the Chensilou Coal Mine in China. Based on systematic observations and analysis of the geological and hydrogeological conditions in the study area, this study conducts theoretical analyses, numerical simulations, and underground observations in a comprehensive manner. Accordingly, a systematic and substantive investigation of the deformation and failure of the deep mining floor and the water inrush mechanism (i.e., the high hydraulic pressure within ash-filled fissures) in the Chensilou Coal Mine is carried out. The burial depth is deeper than 761.4 m, and the water pressure in the limestone of the Taiyuan Formation exceeds 4.95 MPa. Furthermore, the mining depth of the working face is 34.25 m. Based on data on water inrush events and subsurface mining failure depth, the water inrush mechanism in the floor of the coal seam in the Taiyuan Formation is analyzed. The end hole depth of the working face is composed of the L8 limestone, and transient electromagnetic detection technology is used to test the grouting effect of the working face floor and ensure the mining safety of the three working faces tested in this study.

Keywords Deeply buried high-pressure coal seam · Fissure-type water inrush mechanism · Floor failure depth · Treatment practice

Introduction

Water inrush events from limestone aquifers in coal seam floors have become a recurring factor as the coal mining depth has progressively increased, and thus, the mining safety of deep mines has decreased.

An increasing number of researchers have recently studied the damage depths of the floors of deeply buried coal seams with underlying high-pressure limestone aquifers (Chen et al. 2011; Cui 2011; Ge 2011; Guo et al. 2011; Han et al. 2011; Shen and Ran 2013; Zhang et al. 2013; Shi et al. 2014; Song et al. 2014; Li et al. 2015; Lu and Wang 2015; Odintsev and Miletenko 2015; Cheng et al. 2016; Yin et al. 2016; Li et al. 2017). Many scholars (Zhang et al. 2013; Song et al. 2014; Li et al. 2015; Lu and Wang 2015; Odintsev and Miletenko 2015; Cheng et al. 2016; Yin et al. 2016) have used the Fast Lagrangian Analysis of Continua in 3 Dimensions ($FLAC^{3D}$) numerical simulation software package to study the damage depths of the floors of confined water seams. For example, Zhang et al. calculated the stress and position of critical failure in the floor using the semi-infinite body theory combined with the slip-line field theory of plastic deformation to derive a formula capable of calculating the maximum failure depth of the floor (Ge 2011). In addition, on the basis of field measurements and a review of the literature, Xu and Yang analyzed the measured results of 21 floor depths at burial depths greater than 400 m and obtained statistical formulas for the damage depth of a floor under deeply buried conditions using statistical methods (e.g., regression analysis) (Cui 2011). Some scientific and technical researchers have used the transient electromagnetic method (TEM) to detect anomalously water-rich areas in a limestone-confined aquifer

Responsible Editor: Domenico M. Doronzo

✉ Xianzhi Shi
shixianzhcn@126.com

[1] School of Resource and Earth Science, China University of Mining and Technology, Xuzhou 221116, China

in a coal seam floor (Guo et al. 2011; Han et al. 2011; Shi et al. 2014), and the results have provided a scientific basis for the control of limestone floors in mines. For coal seam floors rich in water or associated with the dynamic recharge of limestone aquifers, most mines use floor grouting transformation technology to control damage to the coalbed floor due to water inrush from limestone aquifers (Chen et al. 2011; Shen and Ran 2013; Li et al. 2017). Nevertheless, the research conducted by the abovementioned scholars and field engineering technicians has focused mainly on controlling the limestone water inrush damage to the coalbed floor and has thus failed to comprehensively investigate the water inrush phenomena and the treatment technologies for deeply buried high-pressure coal seams.

In North China, as coal mining deepens, water inrush events from limestone aquifers in coal seam floors have become an important and decisive factor restricting the sustainable development of coal mines; furthermore, water inrush events exert a negative influence on the regional natural environment, living environment, and tourism resources (Cetin 2018; Cetin et al. 2018). In this region, Carboniferous and Permian strata are the main coal-bearing strata. The Carboniferous and Ordovician limestone underlying the Permian coal seams comprise a regionally strong aquifer that serves as the main water source for water inrush events (Feng and Zhou 2010; Qiao et al. 2014; Zhao 2014; Zhang et al. 2015; Huang and Bai 2017). Recently, the depth of coal mining in eastern China has continued to increase, and the unpredictable Carboniferous and Ordovician strata associated with the deeply buried high-pressure coal seam in the Taiyuan Formation have sometimes resulted in water inrush events in the mine floor (Qiao et al. 2014; Zhao 2014; Zhang et al. 2015). Therefore, water inrush events originating from limestone in the coal seam floor have always reduced the safety of mining in this area (Jin 2002; Feng and Zhou 2010). On the basis of previous research, limestone water inrush phenomena continue to occur within the Taiyuan Formation despite the treatment of limestone water damage throughout the Chensilou Coal Mine (Jin 2002; Zhang 2015; Huang and Bai 2017). Regarding the treatment of karst fissure water in the floors of deeply buried high-pressure coal seams, insufficient effective research has been conducted on the depth of the damage to the floor after coal seam mining; as a consequence, the thickness of the effective aquifer in the coal seam floor cannot be determined. Moreover, the thickness of the grouting transformation in the limestone of the coalbed floor is not precisely known, and the end hole distance to the grouted hole is not clear. In addition, safe production in coal mines is restricted by the lack of comparative analyses on the effects of mines on limestone grouting in coal seam floors before and after the grouting transformation.

Therefore, theoretical analyses, numerical simulations, and underground observations of mining wells have been carried out to (1) ensure that water inrush accidents do not occur during the mining process in deeply buried high-pressure coal seams, (2) systematically and substantively investigate the deformation and damage of deep mining floors and the water inrush mechanism associated with a high hydraulic head within ash-filled fractures throughout the Chensilou Coal Mine, and (3) ascertain how to safely mine the two$_2$ coal seam. The results of this paper will provide a useful reference for the prevention of water inrush accidents in coal mining areas with similar geological features.

Project details and analyses of the deformation and damage depth of the bottom plate of the deeply buried working face

Geological and hydrogeological characteristics of the mine

The Chensilou Coal Mine is located in the eastern part of the Yongxia Coalfield north of Yongcheng, Henan Province, at the junction of Henan Province and Anhui Province (see Fig. 1). The geographical coordinates of the mine are 116° 20′ 23″–116° 25′ 19″ E, 33° 57′ 15″–34° 05′ 01″ N, as shown in Fig. 1. The mining area is 12.5 km long from north to south and 5.9 km wide from east to west (E–W), with an area of 62.3937 km^2. The mining elevation ranges from − 300 to − 900 m. The bottom layer of the mine is composed of the following from bottom to top: Middle Ordovician (O_2), Middle and Upper Carboniferous (C_2, C_3), Permian (P), Neogene (N), and Quaternary (Q) sediments (An 2010). The coal-bearing strata are Carboniferous and Permian in age.

The coal-bearing strata in the mining area exhibit a general monoclinic structure, and the strata tend to trend northwest–southeast (NW–SE) and E–W. The shallow ground of the minefield has a dip angle ranging from 16 to 22° and a depth varying from 5 to 10 m. The nearly E–W-trending structure in the mining area is dominated by faults, as well as a fold, and

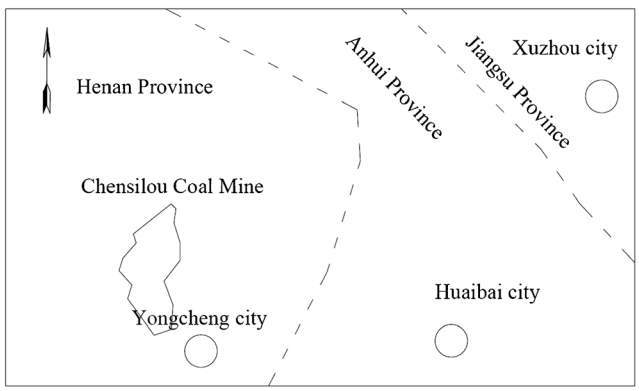

Fig. 1 Location map of the Chensilou Coal Mine

the nearly northeast–southwest (NE–SW)-trending structure is dominated by a fold, as well as a fault (An 2010; Zhang et al. 2013).

The Carboniferous Taiyuan Formation in the minefield contains 11 water-bearing limestone layers, numbered L1–L11 from bottom to top. The sequence of the Taiyuan Formation limestone and its influence on the mining of the two_2 coal seam can be divided into three water-bearing sections: the upper water-bearing section (L8–L11), the central water-bearing section (L4–L7), and the lower water-bearing section (L1–L3). The limestone aquifer group in the upper strata of the Taiyuan Formation is the primary indirect aquifer in the two_2 coal seam. The thicknesses of the limestone layers L11 (layer thickness of 2.0 m) and L8 (layer thickness of 12.8 m) in the upper limestone aquifer group of the Taiyuan Formation are stable (Fig. 2). The original water level elevation was + 28.5~30.2 m. The aquifer unit has a deep-water inflow of 0.113~0.400 L/s•m, and the permeability coefficient is 0.40~1.72 m/day, indicating a moderately water-rich aquifer. Within the Taiyuan Formation, the upper limestone aquifer, which once seriously affected the safe extraction of the two_2 coal seam in this mine, is an important indirect source of water for the two_2 coal seam.

The Ordovician limestone aquifer, which contains thick layers of limestone, is characterized by the development of caves and fissures. The initially observed groundwater level in the Ordovician limestone aquifer was + 28.5 m. The aquifer unit has a deep-water inflow of 1.93 L/s•m and a permeability coefficient of 4.62 m/day, indicating a water-rich aquifer. In the subsurface, the two_2 coal seam is 209.6 m from the Ordovician limestone aquifer. Long-term observations of the mine's ash water level indicate that the Ordovician limestone water can indirectly percolate into the mine through the Taiyuan limestone.

The Chensilou Coal Mine has suffered 11 water inrush accidents since the beginning of production in 1997 (Jin 2002; Zhang 2015; Huang and Bai 2017). Among them, 9 water inrush accidents can be classified as medium- or large-scale water inrush events. The water involved in two of the large-scale water inrush events was sourced from the limestone within the Taiyuan Group.

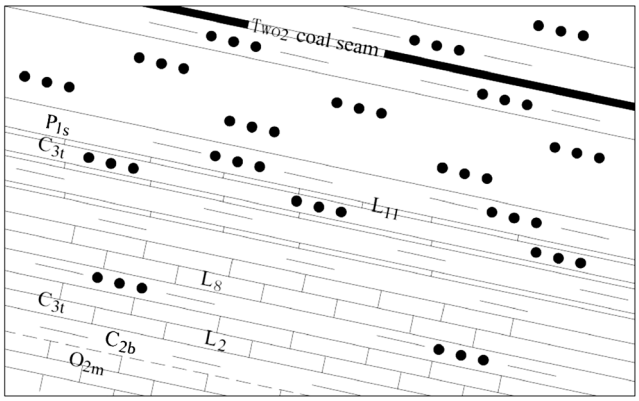

Fig. 2 Two_2 coal seam and the aquifer in its bottom layer. P_{1s}, Permian Shanxi Group; C_{3t}, Carboniferous Taiyuan Formation; C_{2b}, Carboniferous Benxi Formation; O_{2m}, Ordovician Majiagou Formation; L, limestone

Deformation and damage depth analysis

Test work surface overview

The 2517 fully mechanized mining face is located in the fifth mining area of the southern wing of the mine (i.e., the − 720-m horizontal auxiliary mining area). The elevation of the ground above the working face is 32.7~33.8 m, and the working surface elevation is − 696~− 765 m. The slot advancement length along the tracks of the 2517 fully mechanized mining face (upper) is 1284 m, and the slot advancement length along the belt (bottom) is 1300 m; the external eye length of the working face is 126 m, and the endoscopic eye length is 196 m. The northern and southern regions of the 2517 fully mechanized mining face comprise unmined solid coal seams. In contrast, the western region of the working face contains the well boundary and the F38 boundary fault, while the eastern part of the working face contains the − 720-m horizontal auxiliary alley.

The water level of the limestone aquifer in the upper part of the Carboniferous Taiyuan Formation near the 2517 fully mechanized mining face is approximately 201 m, and the hydraulic head pressure of the upper section of the Taiyuan Formation in the 2517 fully mechanized mining face is 4.95~5.64 MPa.

Damage evolution characteristics of the working face plate

(1) Theoretical calculation of the fracture depth of the coal seam floor. When the dynamic stress distributed across the coal seam floor exceeds the ultimate compressive strength of the rock layer composing the coal seam floor, the rock layer undergoes creep deformation, and a plastic deformation failure zone forms in the area where the stress is concentrated. The stress relief zone is within the goaf area, which is subjected to less stress than the area of concentrated stress in front of the work surface. A certain free surface is present, and the creeping rock mass moves towards the goaf area. Plasticity theory states that the plastic deformation range can be divided into three regions: the active stress zone in the first region, the transition zone in the second region, and the passive stress zone in the third region (Yang 2010). The damage depth of the mining floor can be derived according to the shaping theory. The average height M of the two_2 coal seam in the 2517 fully mechanized coal mining face is 2.63 m, the average depth H of the coal seam in the working face is 761.4 m, the average bulk density γ of the overlying strata of the coal seam

is 2500 kg/m^3, the internal friction angle φ_0 of the rock in the two$_2$ coal seam of the working face is 54°, and Poisson's ratio μ is 0.22. These parameters are substituted into the fracture depth formula of the coal seam floor:

$$D_{\mathrm{m}} = \frac{x_\alpha \cos\varphi_0}{2\cos\left(\frac{\pi}{4}+\frac{\varphi_0}{2}\right)} e^{\left[\left(\frac{\pi}{4}+\frac{\varphi_0}{2}\right)\tan\varphi_0\right]} \quad (1)$$

$$x_a = \frac{M}{F}\ln(10\gamma H) \quad (2)$$

$$F = \frac{K_1-1}{\sqrt{K_1}} + \left(\frac{K_1-1}{\sqrt{K_1}}\right)^2 \arctan\sqrt{K_1} \quad (3)$$

$$K_1 = \frac{1+\sin\varphi_0}{1-\sin\varphi_0} \quad (4)$$

where D_{m} represents the maximum damage depth of the bottom plate (m), H represents the coal seam depth (m), φ_0 represents the internal friction angle of the coal floor rock (°), x_a represents the length of the coal yield zone (m), M represents the coal seam mining height (m), and γ represents the average bulk density of the overlying strata in the coal seam (kg/m^3).

Based on a calculation, the damage depth of the coal seam floor in the 2517 fully mechanized coal mining face of the Chensilou Coal Mine is 28.1 m. This value is much larger than that (14.7 m) reported by Zhang et al. (2015) for a coal seam at a burial depth of 466 m.

(2) Numerical simulation of the damage depth of the floor of the deeply buried working face based on FLAC^{3D}. FLAC^{3D} software is used mainly for the computer simulation of mechanical problems encountered in geology, geomechanics, and mining engineering. This study uses Lagrangian software to simulate the damage depth of the coal seam floor (Cui 2011).

According to the actual situation of the 2517 fully mechanized mining face, the inclined length of the simulated working face in the research project is 150 m, the advancement length is 600 m (the actual simulated advancement length is 500 m), the thickness of the two$_2$ coal seam is 2.6 m, the dip angle of the simulated rock is approximately 6°, and the overburden thickness is 135 m. The compositions of the top and bottom plates of the working face are shown in Fig. 3. The total mine height is adopted for the working face, and the roof is modeled via comprehensive collapse management (Wang et al. 2011). In the model, the coordinate system is defined as follows: the working surface represents the X axis, the mining direction is the Y axis, and the direction of gravity is the Z axis, with the upward direction considered the positive direction (Fig. 3). The working face is pushed forward by 20 m in the mining direction in every step. A total of 25 steps (i.e., 500 m) are performed in the simulation.

The simulation results show that the damage height of the roof and the depth of the damage to the floor gradually increase with the continuous advancement of the working face. When the working face is mined to 280 m, the height (depth) of the top (bottom) damage level in the coal seam tends to be stable; at this moment, the maximum damage height of the roof is approximately 54 m, and the maximum depth of the damage to the floor is approximately 37 m. Then, the height (depth) damage level in the roof of the working face is basically stable. The simulation results in this study are consistent with those reported in the literature (Zhang et al. 2013; Song et al. 2014; Li et al. 2015), according to which, with an increase in the burial depth, the damage to the bottom plate of the working face deepens. Figure 4 shows the plastic distribution areas in the top and bottom plates when the working face is mined to 20 m, 160 m, 280 m, 320 m, and 500 m.

(3) On-site electric method for detecting the damage depth in the working surface floor. We use high-density resistivity and continuous imaging detection techniques for high-quality drilling with the goals of dynamically monitoring the 2517 fully mechanized mining face and investigating the damage pattern and depth of the working surface floor during the mining process. Therefore, for this project, the WDJD-2 high-density electrical prospecting instrumentation is chosen for continuous borehole detection. The collection of the scientific data is performed using RES2DINV software, and mapping is performed with Surfer8 (Lin et al. 2015).

Three observation holes are designed, constructed, and arranged in three drilling fields along the 2517 belt groove. The observation hole DZK1 (#1) is arranged in the #8 drill field at a distance of 45 m from the cut hole in the 2517 belt, and the final edge of the hole is 60.2 m from the cut hole (Fig. 5). Hole DZK2 (#2) is arranged in the #7 drill field at a distance of 153 m from the cut hole in the 2517 belt, and the final edge of the hole is 93.1 m from the cut hole. Hole DZK3 (#3) is arranged in the #5 drill field at a distance of 405 m from the center of the 2517 belt. The parameters for the observation holes are shown in Table 1.

A signal cable is embedded in each hole, and each cable is connected to 30 electrodes with an electrode spacing of 4 m. Copper ring electrodes and high-strength 32-core cables are used, and the drill holes are plugged with slurry. The amount of deformation is measured by two kinds of alignment devices. The A-MN-B device is configured with 243 measuring points each time, and 27 rolling measurements are performed in 9 sections. The α-arrangement device has 30 electrodes with 135 measurement points each time, and 28 rolling measurements are performed in 9 sections.

From the working face to the mining face, the #3, #2, and #1 boreholes are measured twice over 10 days; then, measurement of the #3 drill field is stopped, and the #2 and #1 boreholes are observed every 2 days. When the mining face reaches the #1 borehole, one measurement per week is acquired in the #3 borehole; at this time, the #1 and #2 boreholes are measured once every 3 days. When the mining face reaches the #3 borehole, the #1 and #2 boreholes are measured once a week, and the #3 borehole is measured once every 3

Stratigraphic unit	Stratum thickness (m)	Column	Rock name
P_{lx}	7.91		Bauxitic mudstone
P_{ls}	25.83		Sandy mudstone
	12.69		Mudstone
	9.29		Fine-grained sandstone
	5.96		Sandy mudstone
	2.63		Two_2 coal
	3.75		Sandy mudstone
	11.01		Fine-grained sandstone
	6.13		Mudstone
	8.55		Medium-grained sandstone
	14.20		Sandy mudstone
C_{3t}	1.45		L_{11} limestone

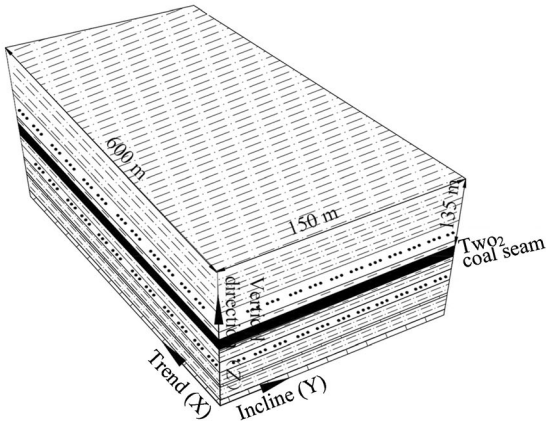

Fig. 3 2517 fully mechanized mining face. Left, the comprehensive stratigraphic column of the top and bottom plates. Right, the 3D model

days. After the mining face has passed the #3 borehole by 50 m, the three boreholes are measured once a week. After the mining face has passed the #3 borehole by 100 m, the three boreholes are measured every 2 weeks. The observations are stopped when the observation data stabilize. After stabilization, the apparent resistivity profile of the #2 borehole floor is measured, as shown in Fig. 6. The curves of the #2 borehole depth and the floor damage depth are shown in Fig. 7.

The results of the high-density electrical field observations for boreholes #2, #1, and #3 were analyzed comprehensively to ascertain the relationship between the working face advancement length and the floor damage depth, as shown in Fig. 8.

After analyzing the inversion results of boreholes #2, #1, and #3 (based on the visible resistivity profile and damage depth profile), the maximum damage depth to the bottom plate of the 2517 fully mechanized mining face is considered to be approximately 40.75 m. However, after the bottom plate is collapsed and pressed to achieve secondary stability, the depth of the damage to the bottom plate is stable at 34.25 m. Nevertheless, due to the great burial depth, the measured damage depth of the floor of the working face is larger than that reported in the literature (Xu and Yang 2013; Shi et al. 2014); therefore, the obtained data are of practical significance.

Determining the damage depth of the floor of the 2517 fully mechanized mining face

Through theoretical calculations of the depth of the damage to the floor in the deeply buried 2517 fully mechanized mining face under high-pressure conditions, the results from $FLAC^{3D}$ numerical simulations, the high-density electrical analysis of the underground site, the deformation and damage evolution characteristics, and the depth of the working face are collectively employed to perform a comprehensive analysis. Accordingly, the damage depth during coal mining to the coal seam floor under deeply buried and high-pressure water conditions is obtained. According to the comprehensive analysis, the maximum damage depth of mining activity in the 2517 fully mechanized mining face is 40.75 m under deeply buried

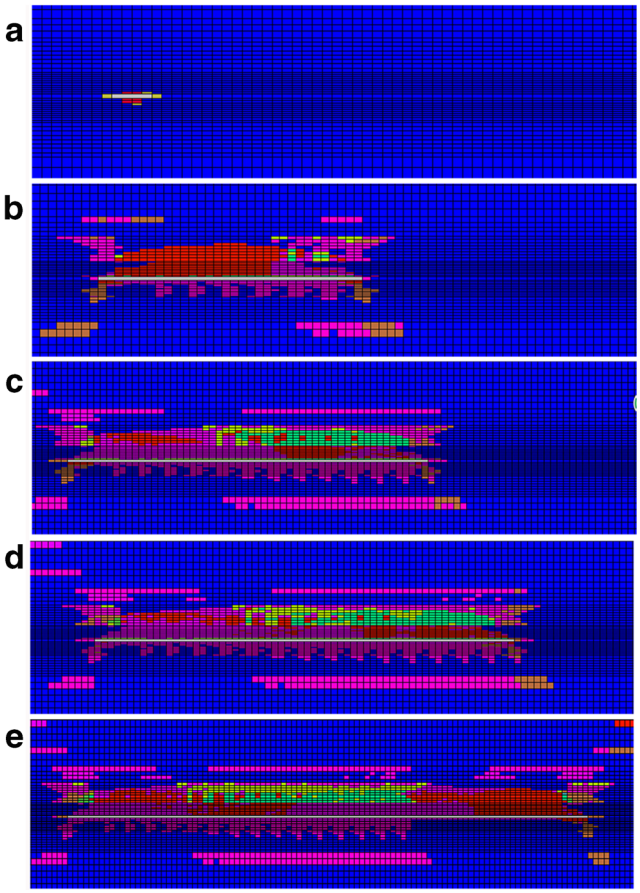

Fig. 4 Plastic distribution areas of the top and bottom plates when the working face is mined to 20 m, 160 m, 280 m, 320 m, and 500 m. **a** 20 m. **b** 160 m. **c** 280 m. **d** 320 m. **e** 500 m

and high-pressure water conditions. However, after the coal seam roof collapses and the bottom plate is pressed to achieve secondary stability, the damage depth of the bottom plate is 34.25 m.

Water inrush mechanism in the floor fissures of a deeply buried high-pressure coal seam

Through an analysis of the geological and hydrogeological conditions of the study area and the water inrush data acquired from the Chensilou Coal Mine over many years, the effects of water inrush damage and the restrictions on safe production in the study area are mainly believed to be the result of karst fissure water in the upper limestone aquifer in the two$_2$ coal seam floor of the Taiyuan Formation. Under the action of surface stresses during mining, the activation of the primary crack in the bottom plate and the expansion of the mining fissure provide the main passages for flow by connecting the water in the Taiyuan Formation limestone with the stope. However, no fault structure that could be regarded as the primary water-guiding channel caused by the expansion of fractures via mining has been found in the main water inrush location in the Chensilou Coal Mine. Therefore, on the basis of summarizing the geological and hydrogeological conditions of the study area, further analyses of the fissure-type water inrush mechanism in the coal seam floor of the Taiyuan Formation should focus on the expansion of the fracture caused by crack propagation during mining.

Model development

According to the deformation characteristics during the evolution of the mining floor failure of the 2517 fully mechanized mining face, the stress state of the coal and rock masses around the stope changes with increasing distance to the working face. The secondary stress above the coal pillars on both sides of the face gradually increases; simultaneously, the disturbance to the floor gradually increases, which causes the degree and depth of damage in the floor (within a certain range of the goaf area and its two sides) to gradually increase. The floor in the middle part of the goaf area is subjected to tensile deformation due to pressure relief, while the coal seam pillars on both sides are deformed by shear due to secondary mining stresses and are generally inverted in a saddle shape. In addition, the secondary stress also strengthens the water-rock effect of the high-pressure aquifer below the floor. On the basis of the height of the original guiding fracture, some weak cracks gradually develop upwards, forming a secondary fracture surface. Therefore, the general mode of expansion for the ash-fissure-type water inrush mechanism can be established in the deeply buried coal seam floor of the Chensilou Coal Mine, as shown in Fig. 9.

Figure 9 shows that as the working surface advances, the thicknesses of the water barrier layer (M) and the original guiding zone (h_0, which is generally not large (part of the position is equal to 0 and negligible)) remain unchanged, but as the damage depth in the floor (H_1, H_2…) gradually increases, the thickness (M_1) of the effective aquifer gradually decreases. The height (h_1, h_2…) of the fracture surface within the high-pressure Taiyuan Formation limestone aquifer also gradually increases along the fracture surface. When the height of the fracture surface in the secondary fracture zone reaches the floor of the damage zone (i.e., after the two fractures become connected), a fracture-type water inrush accident occurs in the limestone aquifer in the Taiyuan Formation.

In conjunction with Fig. 9, the three theoretical and generalized conditions for the risk of water inrush phenomena in the study area are as follows:

$$\textit{Water inrush critical conditions}: \quad M_1 = h_2 + h \tag{5}$$

$$\textit{Nonwater inrush condition}: \quad M_1 > h_2 + h \tag{6}$$

$$\textit{Water inrush condition}: \quad M_1 < h_2 + h \tag{7}$$

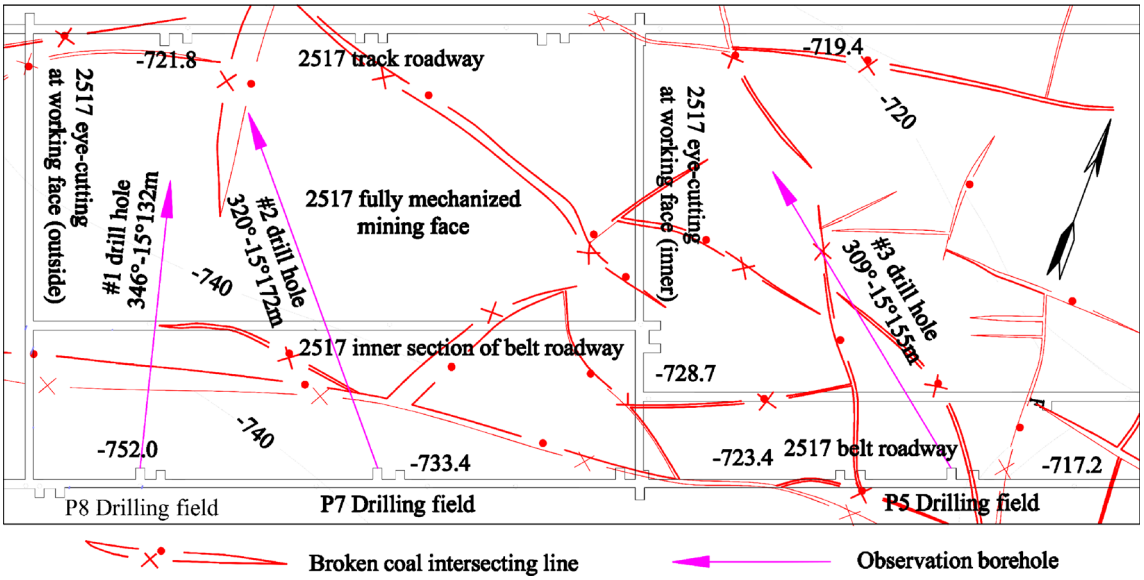

Fig. 5 Arrangement of the observation holes for determining the mining failure depth of the 2517 fully mechanized mining face

where the effective aquifer thickness (M_1) can also be approximated as follows if h_0 is generally not large:

$$M_1 = M - H_2 - h_2 = M - H_2 - h_2 - h_0 \tag{8}$$

Substituting formula (5) into formula (8) reveals the following:

$$M_1 = M - H_2 - h_2 - h_0 = M - H_2 - (h_2 - h_0) = M - H_2 - M_1$$

We can finally obtain the following formula:

$$M_1 = \frac{1}{2}(M - H_2) \tag{9}$$

There are two kinds of expressions, namely formulas (5) and (9), for the critical conditions after the fracture-type water inrush mechanism of the deeply buried mining floor is generalized. On the basis of the actual situation, two parameters, namely the original riser zone (h_0) and the maximum height of the fracture surface of the high-pressure aquifer (h_2), are generally not easy to obtain, but the thickness of the floor aquifer (M) and the floor failure depth (H_2) can be obtained via drilling and on-site measurements. Both types of data are available in the study area; therefore, the critical conditions therein can be analyzed.

On-site validation

Through theoretical calculations of the damage depth of the coal seam floor in the deeply buried 2517 fully mechanized mining face under high-pressure conditions, the results of FLAC^{3D} numerical simulations, the high-density electrical analysis of the underground site, the deformation and damage evolution characteristics, and the depth of the working face are used to perform a comprehensive investigation. Under the conditions of a deeply buried high-pressure mine, the mining failure depth of the two$_2$ coal seam in the 2517 fully mechanized mining face in the study area is 34.25 m. The distance between the two$_2$ coal seam and the L11 limestone layer is 43.4 m. According to formula (9), the critical value of the effective aquifer thickness between the two$_2$ coal seam and the L11 limestone fractured aquifer in the Taiyuan Formation is approximately 8.15 m. These data are determined by the damage depth of the mining floor and the thickness of the water layer in the coal seam floor. These two types of data display certain differences in different locations throughout the study area. Therefore, the critical thickness of the effective aquifer also fluctuates within a certain range. Mining damage and high-pressure water conditions create the possibility of water inrush events in the coal seam floor of the 2517 fully mechanized mining face; this possibility depends mainly on

Table 1 Design parameters of the belt groove observation holes in the 2517 fully mechanized mining face

Hole number	Orientation (°)	Inclination (°)	Hole depth through the L11 limestone (m)	Design hole depth (m)
#3 observation hole (DZK3)	309	− 20	140	155
#2 observation hole (DZK2)	320	− 15	155	172
#1 observation hole (DZK2)	346	− 15	119	132

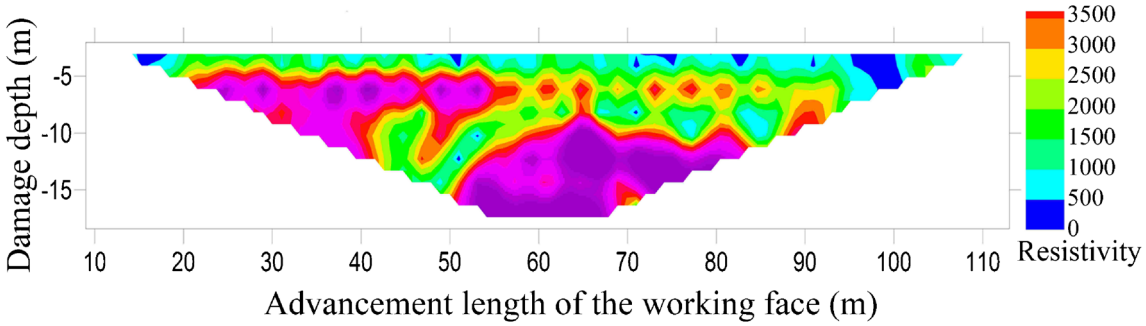

Fig. 6 Profile of the apparent resistivity when the floor of borehole #2 is damaged after stabilization. Field data were collected with a WDJD-2 multifunctional digital direct current instrument (Beijing Tongde, Beijing, China), and 2-dimensional inversion was performed with RES2DINV software

the critical value of the effective aquifer thickness. Therefore, mine production faces a serious water inrush threat in the floor of the 2517 fully mechanized mining face.

Practice for treating substantial fissure water damage in the working face of a deeply buried coal seam floor under high-pressure water conditions

The − 720-m horizontal auxiliary mining area is located in the southern wing of the Chensilou minefield and is situated south of the 15th mining area in the southern wing and the protective coal pillars in the mining area, north of the natural lower boundary of the southern mining area, west of the minefield, and east of the three southern horizontal alleys. The lower limit of the − 720-m horizontal auxiliary mining area is − 860 m, and the upper limit of the area is − 681 m. The elevation of the auxiliary mining area is + 32.7~+ 35.2 m. There are 5 fully mechanized mining faces, namely the 2513, 2515, 2517, 2519, and 2521 fully mechanized mining faces, throughout the − 720 auxiliary mining area in the southern wing. The first face to be produced during the design of the mine was the 2517 fully mechanized mining face, followed by the 2513 and 2515 fully mechanized mining faces.

The water level in the limestone of the Taiyuan Formation in the fifth horizontal auxiliary mining area located south of the mine is − 57.88~− 323.2 m. The hydraulic head pressures in the upper part of the Taiyuan Formation in the floor of the two_2 coal seam in each working face in the study area range from 4.95 to 5.64 MPa. Hence, according to the calculation formula for a safe hydraulic head pressure in a coal mining face ($M = P/TS$), the safe thickness of the aquifer is 77~87 m. Additionally, the depth of the coal seam floor in the working face in this area is 80.3~86.3 m below the two_2 coal seam, and the end of the borehole is in the L8 limestone layer.

Example of water damage prevention in the 2517 fully mechanized mining face

Before the grouting of the bottom plate in the 2517 fully mechanized mining face, an initial TEM survey was performed in the mine along two crossheadings. In this survey, two B-level water-rich anomaly zones and five A-level water-rich anomaly zones were detected, as shown in Fig. 10.

According to the hydrogeological conditions of the working face, in combination with the water-rich anomalies

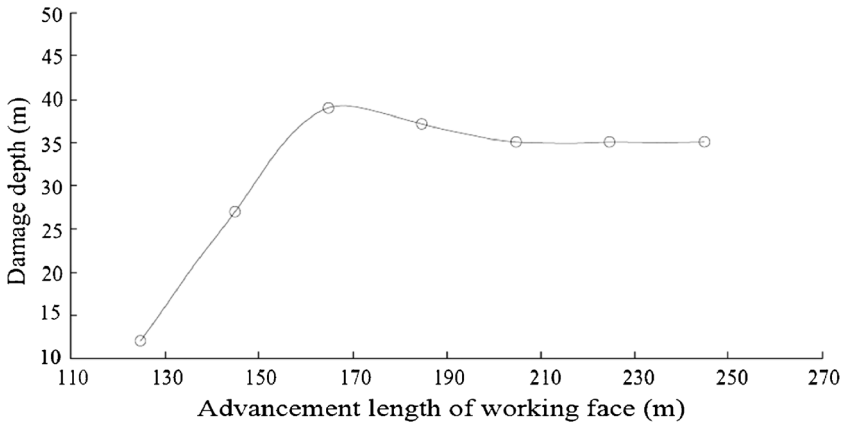

Fig. 7 Relationship between the advancement length of the working face for borehole #2 and the floor damage depth using the high-intensity resistivity method

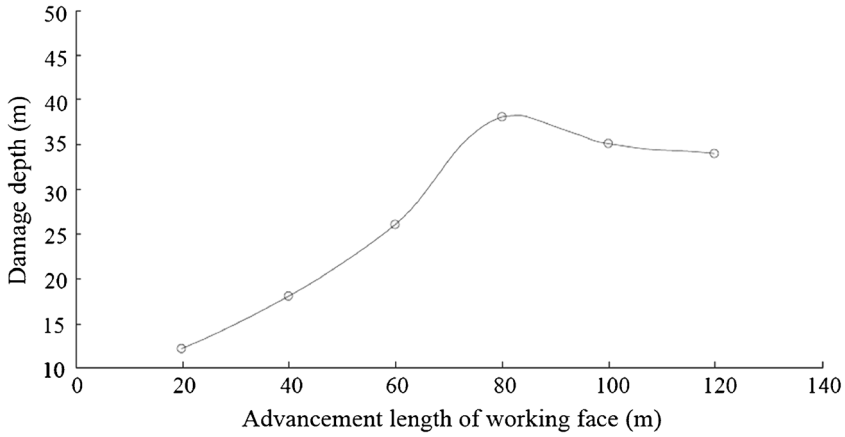

Fig. 8 Relationship between the measured advancement length of the working surface and the floor damage depth based on the high-density electrical field observations for boreholes #1, #2, and #3

detected by TEM, a total of 18 sets of drilling rigs (9 sets of track grooves and 9 sets of belt grooves) were designed for the 2517 fully mechanized mining face. In addition, a total of 381 holes were designed, and the drilling capacity was 55,233 m. In total, 98 drilling holes were inspected, and the total drilling quantity was expected to be 14,108 m.

After the grouting transformation of the bottom plate was carried out, a TEM survey was again performed along the two 2517 crossheadings, and 11 B-level water-rich anomaly zones and 1 A-level water-rich anomaly zone were detected. Among them, the initially detected B1, B2, A2, and A4 water-rich anomalies were not observed, and the A1, A3, and A5 water-poor anomaly areas were reduced, as shown in Fig. 10.

According to the results of the second TEM survey, the drilling area in the surveyed working area containing the abovementioned anomaly areas was verified. A total of 20 verified boreholes were constructed on the working face, and the accumulated water was accessed via 22 drilled holes. The maximum water output per hole was 77 m^3/h, and the total grouting amount was 896 t. The grouted boreholes indicated that two water-rich anomalies, B4 and B9, were well developed and that these water-rich anomalies were relatively strong. After implementing grouting reinforcement, the boreholes P5 plus 3 and WP2 plus 2 were added; then, the B4 and B9 water-rich anomalies were inspected again and further grouted. The water outputs of these two boreholes were 3

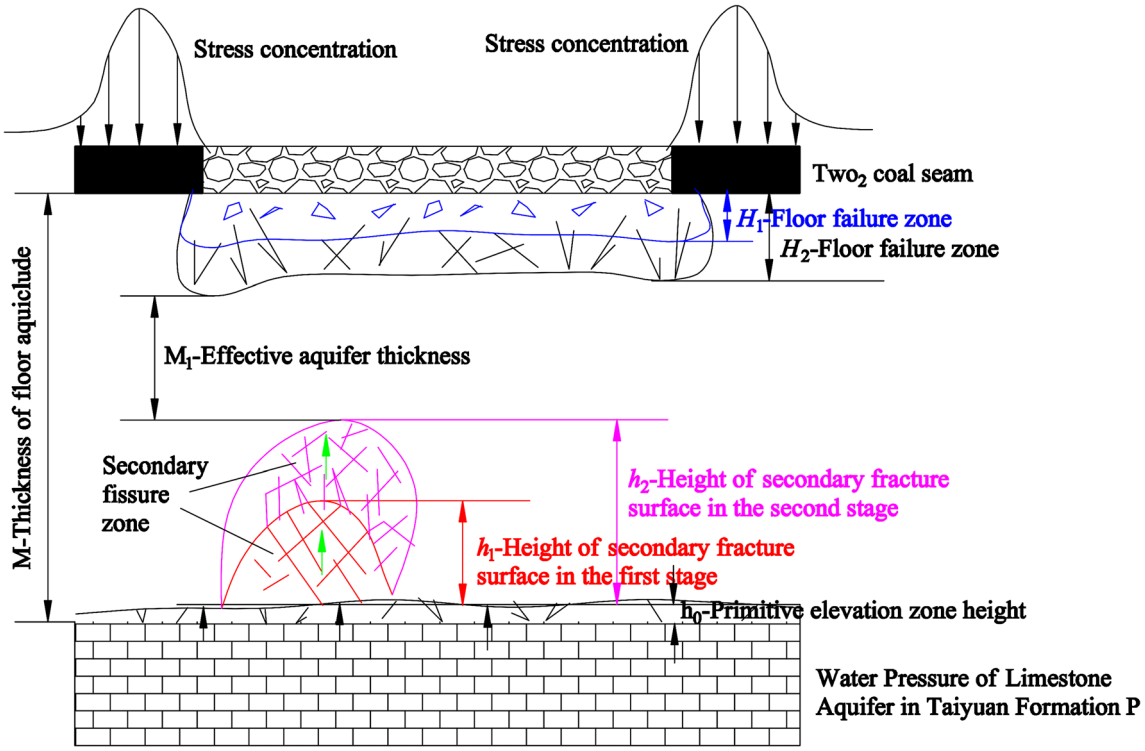

Fig. 9 Fracture-type water inrush mechanism for the floor of a deeply buried mine

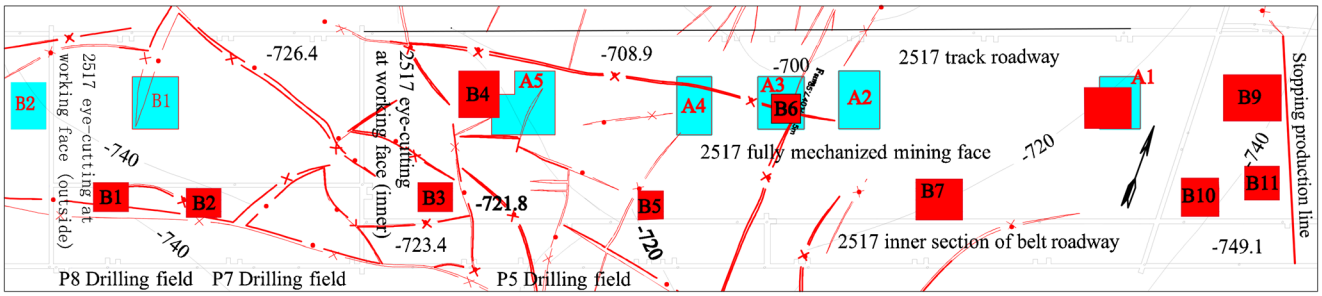

Fig. 10 Distribution map of the reassessed water-rich anomaly area after grouting the 2517 fully mechanized mining face. Blue areas represent the preliminary water-rich anomaly areas, and red areas represent the resurveyed water-rich anomaly areas

m^3/h and 2 m^3/h, respectively, proving that good grouting transformation effects had been established in the B4 and B9 water-rich anomaly areas.

A total of 388 holes were drilled and rebuilt in the 2517 fully mechanized mining face: the total length of drilling was 61,405.5 m, and the total grouting amount was 31,722.2 t. Among the drilled boreholes, 105 boreholes were tested (including the water-rich anomaly zone detected by TEM before grouting and the grouted boreholes and water-rich anomaly zones detected after grouting). The total length of drilling was 20,327 m, and the grouting amount was 8129.6 t. The average single-hole grouting amount in the 2517 fully mechanized mining face was 82 t/hole, and the grouting amount per square meter in the coal seam floor was 0.136 t. Through grouting reinforcement, the effect of the bottom plate transformation was good, thereby ensuring the safe recovery of the working face.

Example of water damage prevention in the 2513 fully mechanized mining face

Before floor grouting reinforcement was performed on the 2513 fully mechanized mining face, a TEM survey was conducted in the mine, and two A-level and two B-level water-rich anomalies were detected (Fig. 11).

According to the hydrogeological conditions of the working face in combination with the water-rich anomaly detected by TEM, 14 sets of drilling rigs (5 sets of track grooves and 9 sets of belt grooves) were designed for the grouting reinforcement of the 2513 fully mechanized mining face. In the 182 construction holes, the total grouting amount was 16,990.52 t, and the total length of drilling was 28,973.5 m. In the grouting process, 6 drilling holes were arranged in the A1 water-rich anomaly zone, where the cumulative amount of grouting was 191.25 t; 6 drilling holes were arranged in the B1 water-rich anomaly zone, where the cumulative amount of grouting was 85 t; 10 drilling holes were arranged in the A2 water-rich anomaly area, where the cumulative amount of grouting was 505.9 t; and 3 drilling holes were arranged in the B2 water-rich anomaly, where the cumulative amount of grouting was 177 t.

After grouting and reinforcing the working surface floor, the grouting effect of the mine in the 2517 two-slot groove was reassessed by a TEM survey, and no water-rich anomaly areas were detected in the working floor.

Example of water damage prevention in the 2515 fully mechanized mining face

Before grouting the floor of the 2515 fully mechanized mining face, an initial TEM survey was conducted in the two crossheadings, and 8 B-level water-rich anomaly zones and 4 A-level water-rich anomaly zones were detected (Fig. 12).

After the grouting transformation of the bottom plate, another TEM survey was conducted in the two crossheadings of the 2515 fully mechanized mining face, and 12 B-level water-

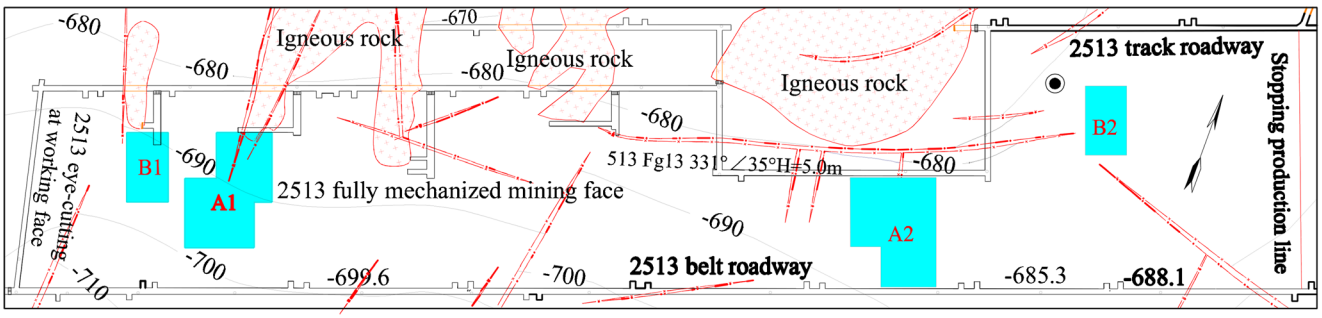

Fig. 11 Preliminary distribution diagram of the water-rich anomaly zones before grouting the 2513 fully mechanized working face. Blue areas represent the initial water-rich anomaly zones

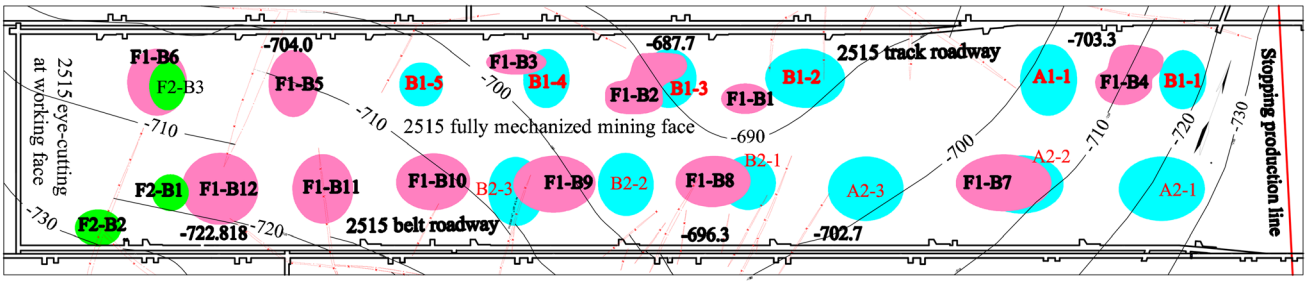

Fig. 12 Distribution of water-rich anomaly zones after the second TEM survey of the 2515 fully mechanized working face. Blue areas represent the initial water-rich anomaly zones, red areas represent the results of the first TEM survey of the water-rich anomaly zones, and green areas represent the results of the second TEM survey of the water-rich anomaly zones

rich anomaly zones were detected, while no A-level water-rich anomaly zones were found. The water-poor anomalies in the B1–1, B1–2, B1–5, B2–2, A1–1, A2–1, and A2–3 zones detected during the first survey were excluded from being water-rich anomalies, and the ranges of the B1–3, B1–4, B2–1, B2–3, and A2–2 water-rich anomalies were reduced.

Twelve water-rich anomalies were discovered by TEM after grouting reinforcement of the working surface floor. The mine redesigned and regrouted the floor and then reassessed the floor grouting borehole using TEM. The second TEM survey detected three B-level water-rich anomaly zones and no A-level water-rich anomaly zones. The F1–B1, F1–B2, F1–B3, F1–B4, F1–B5, and F1–B7~F1–B12 water-rich anomaly regions detected in the first survey were no longer observed, and the range of the F1–B6 water-rich anomaly zone was reduced.

A total of 338 drilling holes were drilled in the 2515 working face; the total length of drilling was 52,728.7 m, and the total grouting amount was 22,584.7 t. Among these holes, 189 holes were inspected (including boreholes in water-rich anomaly areas identified via the TEM survey before grouting, grouting boreholes and boreholes in water-rich anomaly areas detected after grouting). For the inspected holes, the total length of drilling was 27,783 m, and the grouting amount was 6051.2 t. The average single-hole grouting amount in the 2515 working face was 66.8 t/hole.

Conclusion

(1) This paper selects a deeply buried coal seam floor and high-pressure fully mechanized mining face in typical North China strata as the research object and obtains the evolutionary characteristics of the floor damage depth during the coal seam mining process under deeply buried, high-pressure water conditions. The damage depth of the floor of the deeply buried coal seam is determined to be 34.25 m.

(2) The end hole horizon of the grouting borehole in the floor of the high-pressure working face is optimized and determined to be the L8 limestone of the Taiyuan Formation.

(3) The water inrush mechanism is found to be the expansion of fissures in the floor of the coal seam under high-pressure conditions. The concepts of water inrush phenomena and high-hydraulic-pressure aquifer fissures are analyzed in combination with the damage subjected to the mining floor under high-stress and high-water-pressure conditions, and the proposed expression for the effective aquifer thickness under critical water inrush conditions is $M_1 = 1/2(M - H_2)$.

(4) Through the treatment of the limestone floors of deeply buried, high-pressure fully mechanized coal mining faces, water damage prevention and control technology models for the Taiyuan Formation limestone, which experiences high-pressure fissure-type water inrush events in the coal seam floor, have been established by strictly determining the hydraulic head of the floor aquifer of the working surface and then empirically determining the depths of the coal seam floor and the transformation horizon. The mining working face is detected by TEM, and the grouting drilling design of the working surface floor is modified in a targeted manner. The effect of the transformation of the working face was detected by TEM surveying to determine the effect of grouting, and follow-up TEM surveys were performed to ascertain the changes in the initially detected water-rich anomaly zones. The water-rich anomaly zones detected by TEM are drilled and verified and then further grouted to generate transformations. The drill holes are checked again to verify the water-rich anomaly zones revealed by follow-up TEM surveying. When the water inflow is verified to be less than 5 m^3/h, the grouting can be stopped, whereas water-rich areas with a water inflow exceeding 5 m^3/h continue to be grouted, and inspections are carried out until the water inflow of each inspection hole is less than the threshold of 5 m^3/h. At present, all three working faces have been safely grouted, and the occurrence of water inrush accidents in the limestone fissured aquifer in the Taiyuan Formation caused by mining the two_2 coal seam under deeply buried and high-pressure water conditions has been prevented.

Compliance with ethical standards

Conflict of interest The authors declare that they have no conflicts of interest.

References

An K (2010) Study of the floor failure and water-inrush prediction of Chensilou Coal Mine. Dissertation, Shandong Univ. Sci Technol

Cetin M (2018) Determination of bioclimatic comfort areas in landscape planning: a case study of Cide Coastline. Turk J Agric-Food Sci Technol 4:800–804

Cetin M, Zeren I, Sevik H, Cakir C, Akpinar H (2018) A study on the determination of the natural park's sustainable tourism potential. Environ Monit Assess 190:167

Chen CY, Wang JH, Chen YZ (2011) Grouting reinforcement technology for floor limestone under complex hydrogeological conditions. Energy Technol Manag 4:69–71

Cheng T, Guo BH, Wang L, Yang XY (2016) Numerical simulation on water inrush from floor during mining above confined aquifer in Jiulishan coal mine. Electron J Geotech Eng 21:5749–5761

Cui S (2011) Study on the failure law of 9# coal seam floor in Xiandewang Mine. Dissertation, Hebei Engineering University

Feng QY, Zhou L (2010) Simulation of fault effect on mining failure of coal seam floor and its application in water disasters control. Geol J China Univ 16:19–25

Ge SL (2011) Stress field and deformation and failure characteristics of floor under the influence of overlying coal seam mining. Eng Technol 16:325–327

Guo M, Chen X, Liu W, Wang YF (2011) Application of technology combined GIS and transient electromagnetic technique in coal mine water burst prevention — a case of Sihe Coal mine. Int Conf Geoinform 2011:1–5

Han D, Li D, Shi X (2011) Effect of application of transient electromagnetic method in detection of water-inrushing structures in coal mines. Proc Earth Planet Sci 3:455–462

Huang WX, Bai HB (2017) Study on fault activation water-inrush from floor under confined water of Chensilou Coal Mine. Coal Technol 36:204–206

Jin DW (2002) Research status and outlook of water outburst from seam floor in China coal mines. Coal Sci Technol 30:1–4

Li A, Liu Y, Mou L (2015) Impact of the panel width and overburden depth on floor damage depth in no. 5 coal seam of Taiyuan group in Chenghe mining area. Electron J Geotech Eng 20:1603–1671

Li H, Bai HB, Wu JJ, Wang CS, Ma ZG, Du Y, Ma K (2017) Mechanism of water inrush driven by grouting and control measures—a case study of Chensilou mine, China. Arab J Geosci 10:468

Lin Y, Wu T, Pan G, Qin Y, Chen G (2015) Determining and plugging the groundwater recharge channel with comprehensive approach in Siwan coal mine, North China coal basin. Arab J Geosci 8:6759–6770

Lu YL, Wang LG (2015) Numerical simulation of mining-induced fracture evolution and water flow in coal seam floor above a confined aquifer. Comput Geotech 67:157–171

Odintsev VN, Miletenko NA (2015) Water inrush in mines as a consequence of spontaneous hydrofracture. J Min Sci 51:423–434

Qiao W, Li W, Zhang X (2014) Characteristic of water chemistry and hydrodynamics of deep karst and its influence on deep coal mining. Arab J Geosci 7:1261–1275

Shen B, Ran DL (2013) Comprehensive prevention and control technology of confined water in Chensilou Coal Mine. Inner Mong Coal Econ 6:63–64

Shi XZ, Zhang JL, Jiang ZQ, Fu XL (2014) Study of mechanized mining face floor limestone water treatment technology in Chensilou Coal Mine. Coal Technol 33:172–174

Song CJ, Fan C, Song L (2014) Study on coal seam mining face floor failure under imbalance high water pressure. Adv Mater Res 919-921:758–761

Wang ZQ, Yang H, Chang YB, Wang P (2011) Research on the height of caving zone and roof classification of mining whole height at one times in thick coal seam. Appl Mech Mater 6:99–100

Xu YC, Yang Y (2013) Applicability analysis on statistical formula for failure depth of coal seam floor in deep mine. Coal Sci Technol 41:129–132

Yang SH (2010) Study on failure characteristics of coal mining floor under pressure on Sunyu Coal Mine. Dissertation, Anhui University of Science and Technology

Yin HY, Lefticariu L, Wei JC, Zhu L, Guo JB, Li ZJ, Guan YZ (2016) A multi-method approach for estimating the failure depth of coal seam floor in a Longwall Coal Mine in China. Geotech Geol Eng 34:1267–1281

Zhang K (2015) Limestone water burst mechanism and prevention technology for fracture coalseam floor in the YongCheng Coalming. Dissertation, China University of Mining

Zhang R, Jiang ZQ, Li XH, Chao HD, Sun Q (2013) Study on the failure depth of thick seam floor in deep mining. J China Coal Soc 38:67–72

Zhang FD, Shen BH, Kang YH (2015) Failure mechanism of coal seam floor an calculation of maximum breaks depth. Min Saf Environ Prot 42:58–61

Zhao QB (2014) Technology of regional advance water prevention and control applied to pressurized coal mining zone above Ordovician limestone karst water. Coal Sci Technol 42:1–4